The short-chain fatty acid acetate modulates epithelial-to-mesenchymal transition

Junfang Lyu[a,b], Mehdi Pirooznia[c], Yuesheng Li[c], and Jianhua Xiong[a,b,*]
[a]Department of Medicine, Division of Endocrinology, Diabetes and Metabolism, Johns Hopkins University School of Medicine and [b]Institute for Fundamental Biomedical Research, Johns Hopkins All Children's Hospital, St. Petersburg, FL 33701; [c]National Heart, Lung, and Blood Institute, National Institutes of Health, Bethesda, MD 20892

ABSTRACT **Normal tissue and organ morphogenesis requires epithelial cell plasticity and conversion to a mesenchymal phenotype through a tightly regulated process—epithelial-to-mesenchymal transition (EMT). Alterations of EMT go far beyond cell-lineage segregation and contribute to pathologic conditions such as cancer. EMT is subject to intersecting control pathways; however, EMT's metabolic mechanism remains poorly understood. Here, we demonstrate that transforming growth factor β (TGF-β)–induced EMT is accompanied by decreased fatty acid oxidation (FAO) and reduced acetyl-coenzyme A (acetyl-CoA) levels. Acetyl-CoA is a central metabolite and the sole donor of acetyl groups to acetylate key proteins. Further, the short-chain fatty acid acetate increases acetyl-CoA levels—robustly inhibiting EMT and cancer cell migration. Acetate can restore EMT-associated α-tubulin acetylation levels, increasing microtubule stability. Transcriptome profiling and flow cytometric analysis show that acetate inhibits the global gene expression program associated with EMT and the EMT-associated G1 cell cycle arrest. Taken together, these results demonstrate that acetate is a potent metabolic regulator of EMT and that therapeutic manipulation of acetate metabolism could provide the basis for treating a wide range of EMT-linked pathological conditions, including cancer.**

Monitoring Editor
Kunxin Luo
University of California, Berkeley

Received: Feb 28, 2022
Revised: Apr 12, 2022
Accepted: May 3, 2022

INTRODUCTION

In 1982, the epithelial-to-mesenchymal transition (EMT) process was experimentally described in embryonic and adult epithelia (Greenburg and Hay, 1982). EMT is initiated by the transforming growth factor β (TGF-β) family of ligands that signals through a family of receptors to alter cell function. During EMT, a polarized epithelial cell loses epithelial features and acquires a spindle-shaped mesenchymal-like cell phenotype (Nieto *et al.*, 2016; Dongre and Weinberg, 2019). TGF-β signaling activates SMAD2 through C-terminal serine phosphorylation (Schmierer and Hill, 2007; Derynck *et al.*, 2021). TGF-β/SMAD2 signaling activates mesenchymal genes (e.g., SNAIL) and represses epithelial genes (e.g., E-cadherin; David and Massague, 2018; Yang *et al.*, 2020). Although evidence has suggested that EMT is associated with diverse biological settings, including embryogenesis (Vicovac and Aplin, 1996), heart development (von Gise and Pu, 2012), organ fibrosis (Iwano *et al.*, 2002; Zeisberg *et al.*, 2007a,b), cancer progression (Ye and Weinberg, 2015), and tumor immune responses (Kudo-Saito *et al.*, 2009; Akalay *et al.*, 2013), the underlying metabolic regulators remain unclear.

Metabolic abnormalities are a hallmark shared by diverse cancer cells (Hanahan, 2022). Mitochondrial fatty acid β-oxidation (FAO) plays a crucial role in the survival of metabolically stressed cancer cells (Schafer *et al.*, 2009). FAO degrades long-chain fatty acids to generate ATP and acetyl-coenzyme A (acetyl-CoA). Acetyl-CoA is a central metabolite that feeds the tricarboxylic acid (TCA) cycle for the catabolic process of energy production but also contributes to anabolic metabolism and lipid synthesis through the action of ATP citrate lyase (ACLY; Houten *et al.*, 2016). Because acetyl-CoA is the sole donor of the acetyl groups for protein acetylation, it operates as a signal transducer (Pietrocola *et al.*, 2015). Altering acetyl-CoA levels can broadly affect gene expression, protein stability, and cell fate and function through protein acetylation (Wellen *et al.*, 2009; Cai *et al.*, 2011; Lee *et al.*, 2014; Xiong *et al.*, 2018). Because the

This article was published online ahead of print in MBoC in Press (http://www.molbiolcell.org/cgi/doi/10.1091/mbc.E22-02-0066) on May 11, 2022.

*Address correspondence to: Jianhua Xiong (jxiong10@jhmi.edu).

Abbreviations used: Acetyl-CoA, acetyl-coenzyme A; CPT, carnitine palmitoyltransferase; EMT, epithelial-to-mesenchymal transition; FAO, fatty acid oxidation; PCA, principal component analysis; TGF-β, transforming growth factor β.

short-chain fatty acid acetate can be converted to acetyl-CoA through the action of acyl-CoA synthetase short-chain family member 2 (ACSS2), increasing evidence suggests that supplementing the culture media with the acetate may modulate gene expression, protein stability, and cell fate and function by directly increasing acetyl-CoA levels (Moussaieff *et al.*, 2015; Schoors *et al.*, 2015; Schug *et al.*, 2015; Balmer *et al.*, 2016; Wong *et al.*, 2017; Xiong *et al.*, 2018).

Here, we demonstrate a novel role for acetate in restraining EMT in cancer cells. In particular, we show that TGF-β–induced EMT is accompanied by a reduction in both FAO and acetyl-CoA levels. Furthermore, acetate inhibits EMT and its associated cell migration by increasing acetyl-CoA levels. We further show that acetate modulates EMT through regulation of α-tubulin acetylation, microtubule stability, and cell cycle arrest. Together, these results establish acetate as an important regulator of the EMT process and provides a new therapeutic strategy for a wide variety of cancers.

RESULTS AND DISCUSSION

Induction of EMT is accompanied by a reduction in FAO and acetyl-CoA levels

As TGF-β signaling plays a major role in inducing EMT (Nieto *et al.*, 2016), we established an EMT model by treating A549 human alveolar epithelial cancer cells with TGF-β1. TGF-β1 robustly induced an EMT-associated morphological switch, adopting a more spindle-like mesenchymal appearance (Figure 1A). Along with this switch, TGF-β1 activated its downstream effector SMAD2. The activation was marked by increased SMAD2 phosphorylation (Figure 1B), the mesenchymal marker SNAIL, and decreased epithelial marker E-cadherin (Figure 1, C and D). Upon induction of EMT, TGF-β1 treatment caused a significant decline in the protein and mRNA levels of CPT1A (Figure 1E, and Supplemental Figure S1A) and a modest reduction in CPT2 expression (Supplemental Figure S1B).

The rate-limiting step in FAO is fatty acid transport from the cytosol into the mitochondrial matrix. Carnitine palmitoyltransferase 1 (CPT1), located on the outer mitochondrial membrane, facilitates this transfer, followed by CPT2 conversion on the inner mitochondrial membrane (Figure 1F; Houten *et al.*, 2016). Because CPT1A is an obligate enzyme responsible for long-chain fatty acid transport into mitochondria during FAO (Houten *et al.*, 2016), we evaluated FAO response in these cells. Untreated A549 cells responded to an exogenous palmitate challenge with an increased oxygen consumption rate, while induction of EMT by TGF-β treatment tended to inhibit FAO (Figure 1G). To confirm these results, we used FAOBlue, a newly designed fluorescent dye (Uchinomiya *et al.*, 2020), to visualize FAO activity in live A549 cells. Consistent with our oxygen consumption rate–based FAO assay results, FAO activity declined in A549 cells following TGF-β treatment and EMT, evidenced by lower fluorescence intensity (Supplemental Figure S1, C and D). Our recent work, together with other studies, has shown that FAO is needed to maintain cellular acetyl-CoA levels through mitochondrial TCA cycle activity (Xiong, 2018a). Consistent with this, TGF-β1–dependent induction of EMT reduced acetyl-CoA levels (Figure 1H). These results suggest that induction of EMT is accompanied by a reduction in FAO and acetyl-CoA levels.

Acetate inhibits EMT by increasing acetyl-CoA levels

Because altered acetyl-CoA levels affect cell fate and function (Xiong *et al.*, 2018), we asked whether a reduction in acetyl-CoA levels could stimulate EMT. To lower acetyl-CoA levels, we used a specific ACLY chemical inhibitor and found that treatment of A549 cells with this inhibitor SB-204990 induced EMT (Supplemental Figure S1, E–G). We next asked whether restoring acetyl-CoA levels could prevent cells from undergoing EMT. We overexpressed CPT1A protein using a heterologous promoter in A549 cells (Supplemental Figure S1H). Constitutive expression of CPT1A mildly increased cellular acetyl-CoA levels (Supplemental Figure S1I), inhibiting the induction of EMT mesenchymal markers following TGF-β1 treatment (Supplemental Figure S1J).

Acetate supplementation in cell culture can replenish acetyl-CoA pools (Figure 2A; Xiong *et al.*, 2018). Therefore, we asked whether acetate treatment could increase acetyl-CoA levels in A549 cells. Surprisingly, acetate treatment increased acetyl-CoA levels in A549 cells more robustly than in CPT1A overexpression (Figure 2B and Supplemental Figure S1I). We reasoned that acetate might play an essential role in the EMT process. Consistent with this idea, we found that acetate supplementation prevented A549 cells from adopting a more mesenchymal-like appearance (Figure 2C).

Acetate-treated A549 cells showed suppressed SMAD2 phosphorylation but did not change SMAD1/5 phosphorylation (Figure 2D and Supplemental Figure S2, A and B), suggesting that acetate treatment decreased EMT-associated TGF-β1/SMAD2 signaling. Acetate treatment also restored the expression of epithelial markers and reciprocal down-regulation of mesenchymal markers (Figure 2, E and F). Confocal laser scanning microscopy confirmed these results. Upon EMT induction, epithelial marker E-cadherin disappeared, and acetate supplementation led to increased E-cadherin (Figure 2, G and H). During EMT, loss of E-cadherin can facilitate cell migration by breaching the basement membrane and switching intermediate filaments, respectively (Nakaya *et al.*, 2008; Eckert *et al.*, 2011). Therefore, we assessed the migratory capacity of acetate-treated cells using a cell culture model of a wound-healing assay. Treatment of A549 cells with TGF-β1 resulted in increased cell mobility, while acetate inhibited this effect (Figure 2, I and J). Similar results were obtained in human pancreatic epithelial cancer cells PANC-1 (Supplemental Figure S2, C–J). These results suggest that acetate supplementation can restore acetyl-CoA levels and inhibit EMT transition.

Acetate regulates EMT-associated α-tubulin acetylation and microtubule stability

Altering acetyl-CoA levels can broadly affect cell fate and function by influencing protein acetylation (Xiong *et al.*, 2018). Therefore, we reasoned that increasing acetyl-CoA levels by exogenous acetate supplementation might modulate EMT-associated protein acetylation. Loss of α-tubulin acetylation leads to microtubule destabilization, potentiating EMT (Gu *et al.*, 2016). Therefore, we hypothesized that acetate might inhibit EMT by contributing to the acetylation of α-tubulin. Our Western blot data confirmed that A549 cells undergoing EMT showed a significant decrease in α-tubulin acetylation levels, which was restored by acetate (Figure 3A). In accordance with these findings, our confocal microscopic analysis showed that inducing EMT in A549 cells reduced acetyl-α-tubulin levels, while acetate treatment rescued acetyl-α-tubulin levels (Figure 3, B and C). Moreover, the long fibers of α-tubulin disassembled into shorter units in A549 cells undergoing EMT, while acetate supplementation enhanced microtubule polymerization (Figure 3, B and C). Because acetylation of α-tubulin contributes to α-tubulin polymerization, stabilizing microtubules (Yun *et al.*, 2021), we asked whether acetate might play a role in α-tubulin polymerization and microtubule stabilization. Our microtubule stability assay showed that the microtubules of A549 cells undergoing EMT were markedly less polymerized (Figure 3, D and E). Acetate treatment caused a dramatic

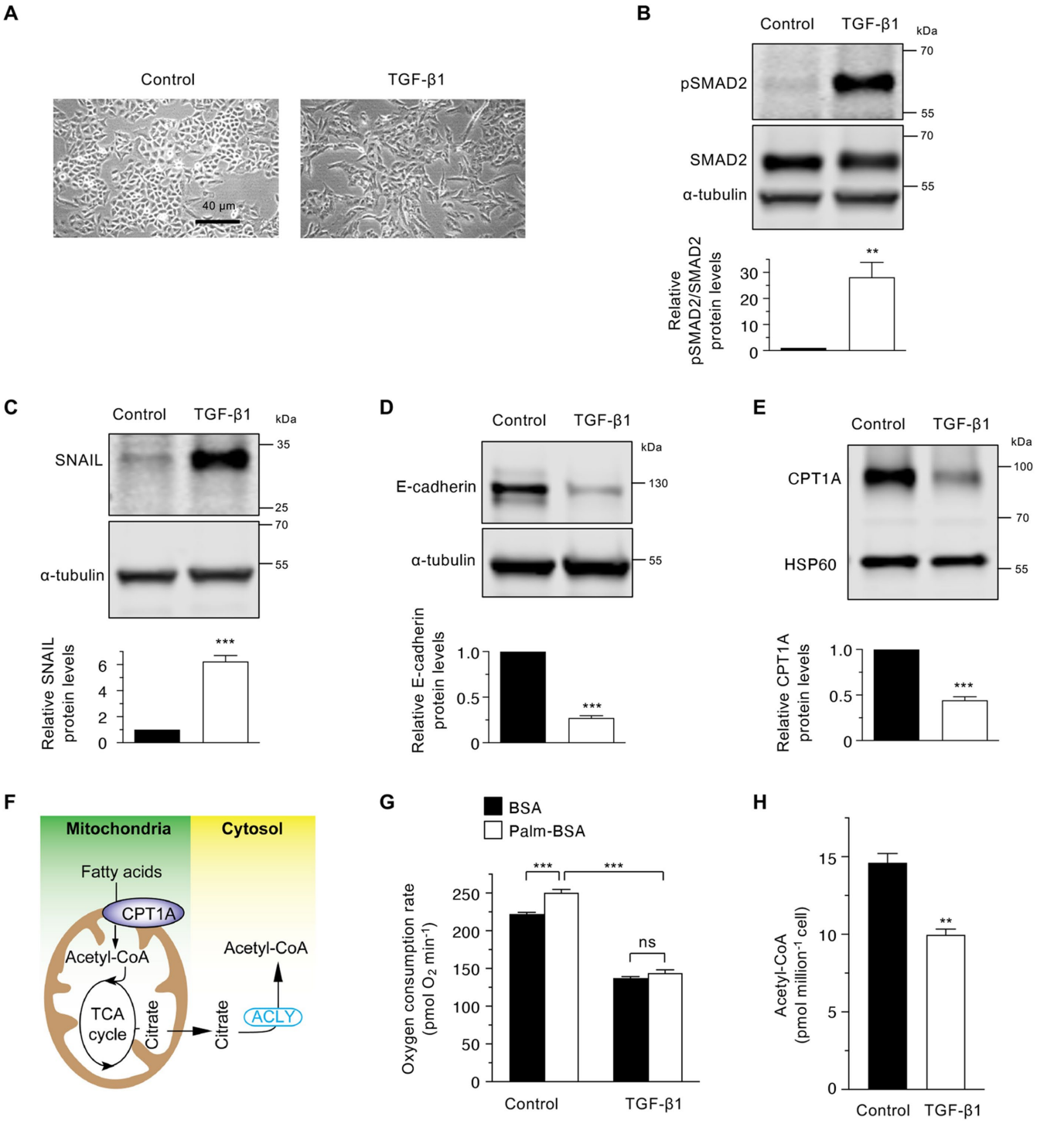

FIGURE 1: EMT induction is accompanied by FAO inhibition and a fall in acetyl-CoA levels. (A) TGF-β1 induces morphological changes consistent with EMT in A549 cells. Scale bar, 40 μm. (B) Western blot analysis of SMAD2 phosphorylation at Ser465/467 in control or TGF-β1–treated A549 cells ($n = 3$ experiments). (C, D) TGF-β1 up-regulates SNAIL (C) and down-regulates E-cadherin (D) ($n = 3$ experiments). (E) TGF-β1 treatment down-regulates CPT1A protein ($n = 3$ experiments). (F) A model for how FAO generates acetyl-CoA through the action of CPT1A. (G) TGF-β1 treatment suppresses FAO, per inability of palmitate conjugated BSA to stimulate OCR ($n = 9$ technical replicates per condition; data = one representative experiment of three similar independent experiments). (H) TGF-β1 treatment reduces acetyl-CoA levels ($n = 3$ experiments). Data represent mean ± SEM and significance via one-way ANOVA with Tukey's multiple comparison test (G). **, $p < 0.01$; ***, $p < 0.001$; ns, not significant.

increase in α-tubulin polymerization and microtubule stability, consistent with acetate modulation of α-tubulin acetylation (Figure 3, D and E).

Epithelial cancer cells from different tissues may share EMT-associated mechanisms underlying α-tubulin acetylation (Gu *et al.*, 2016). Similarly, after TGF-β1 stimulation to induce EMT in PANC-1

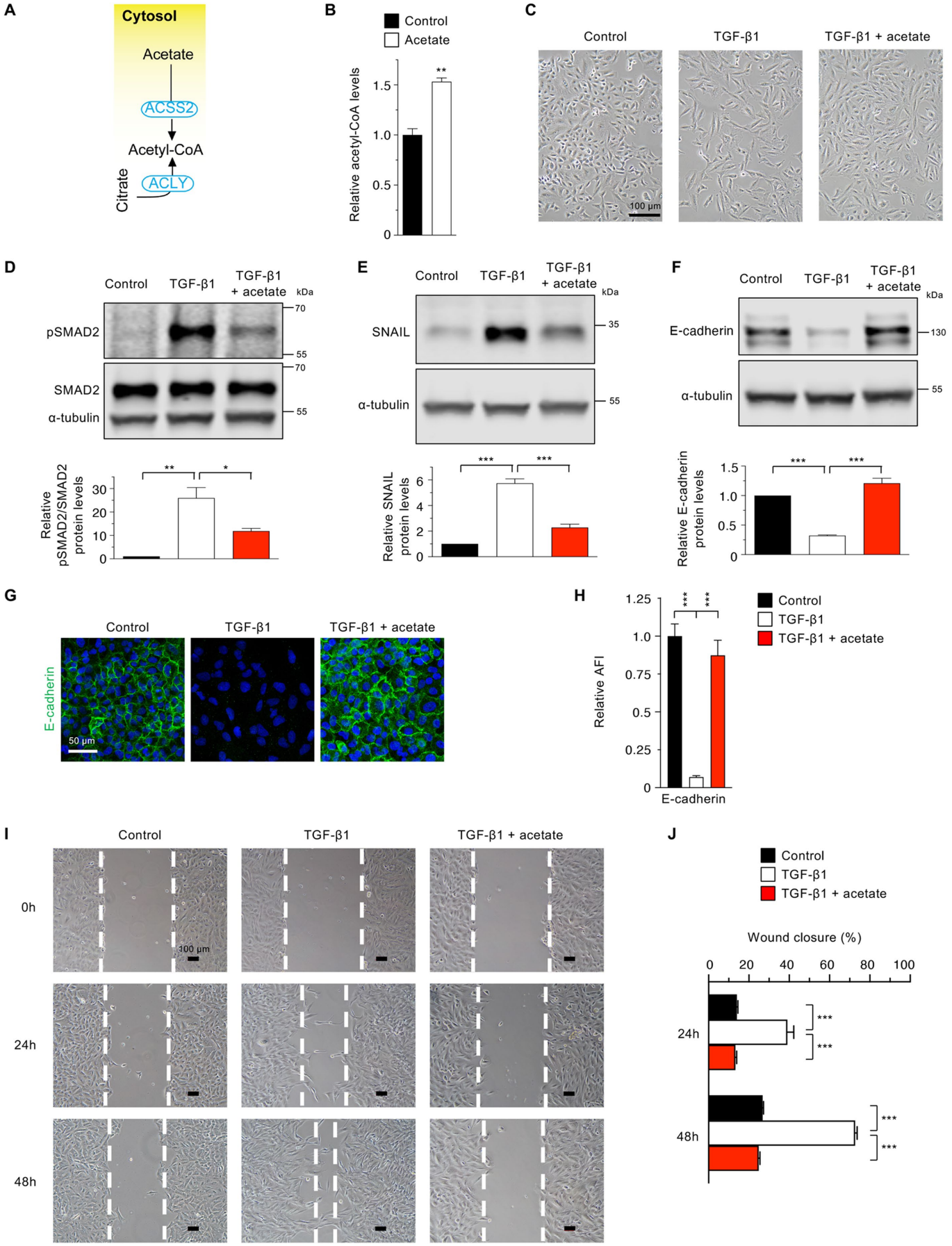
A
Cytosol
Acetate
ACSS2
Acetyl-CoA
Citrate
ACLY
B
Control
Acetate
Relative acetyl-CoA levels
C
Control
TGF-β1
TGF-β1 + acetate
100 μm
D
pSMAD2
SMAD2
α-tubulin
kDa
Relative pSMAD2/SMAD2 protein levels
E
SNAIL
α-tubulin
Relative SNAIL protein levels
F
E-cadherin
α-tubulin
Relative E-cadherin protein levels
G
E-cadherin
50 μm
H
Relative AFI
E-cadherin
I
0h
24h
48h
100 μm
J
Wound closure (%)

and NMuMG, acetate treatment restored α-tubulin acetylation and increased microtubule stability (Figure 3, F–J, and Supplemental Figure S3, A and B). To further assess whether α-tubulin acetylation and microtubule stability play a role in acetate-modulated EMT, we took advantage of acetylation-resistant tubulin mutant K40R and the microtubule destabilizer, vinorelbine. We found that the effect of acetate on EMT is via α-tubulin acetylation and microtubule stability (Supplemental Figure S3, C–E). RNA sequencing (RNA-Seq) analysis of A549 cells showed that acetate treatment inhibited the EMT-specific transcriptomic program (Supplemental Figure S3F). Thus, microtubule stabilization appeared to suppress the EMT program. We obtained similar results using real-time quantitative reverse transcription PCR (qRT-PCR) for select EMT target genes (Supplemental Figure S3, G and H), adding evidence that acetate inhibits EMT. Our results support a role for acetate in mediating microtubule stability and EMT program and provide a potential mechanism linking TGF-β signaling to acetate-mediated microtubule stability.

Acetate inhibits EMT-associated G1 cell cycle arrest

We next asked whether regulation of microtubule stabilization and EMT program by acetate plays a role in EMT-associated cell functions. Because TGF-β signaling potently activates EMT and related cell functions, we reasoned that acetate treatment might modulate EMT-associated cell function. We performed a transcriptome profile in control cells or A549 cells cultured in the presence or absence of acetate following TGF-β1 stimulation. We found that acetate treatment significantly down-regulated the expression of 967 TGF-β1–induced genes (Figure 4A and Supplemental Table S1). Further, principal component analysis (PCA) showed that gene expression changes were more distinct in TGF-β1–treated cells than in control cells. In contrast, acetate treatment prevented EMT-associated gene expression (Figure 4B).

The number of human colorectal cancer cells in the G1 phase increases during the TGF-β1–induced EMT process (Chei *et al.*, 2019), and microtubule depolymerization in human breast cancer cells promotes G1 cell cycle arrest (Blajeski *et al.*, 2002). Consistent with these observations, our gene ontology (GO) analysis pinpointed a significant change for "G1/S transition of mitotic cell cycle" (Figure 4C). A KEGG analysis was consistent with this idea (Figure 4C). Interestingly, key genes associated with G1 cell cycle arrest were regulated by acetate treatment (Figure 4D) and these genes include *CDKN2C* (encoding p18, a specific inhibitor of cyclin-dependent kinase activities required for overcoming G1 checkpoint; Guan *et al.*, 1994; Hirai *et al.*, 1995), *INHBA* (encoding inhibin subunit β A, a member of the TGF-β superfamily of proteins that can induce G1 cell cycle arrest; Jiang *et al.*, 2018), *MCM* family members (*MCM4*, *MCM6I*, and *MCM7* encoding minichromosome maintenance proteins that are key components of the prereplication complex and accumulated during G1 phase; Labib *et al.*, 2001), and *RHOU* (encoding a member of the Rho family of GTPases that contributes to cell accumulation at G1 phase; Canovas *et al.*, 2018). We confirmed acetate-mediated down-regulation of several of these genes by qRT-PCR (Figure 4E). To further investigate the influence of acetate treatment on cell cycle progression, we performed flow cytometric analysis. We found that TGF-β1 treatment arrested the cell cycle in the G1 phase during EMT (Figure 4, F and G), and we reversed this effect by supplementing acetate in culture media (Figure 4, F and G). Furthermore, treatment of A549 cells with the CDK4/6 inhibitor palbociclib acted as an inducer of EMT (Figure 4, H and I). These results suggest that acetate may regulate EMT in a cell cycle–dependent manner.

Our results suggest that acetate can control the EMT process by modulating α-tubulin acetylation, microtubule stabilization, and cell cycle arrest (Figure 4J). Although our data linked acetate to EMT through the regulation of microtubule stabilization and cell cycle arrest, we cannot exclude the possibility that acetate treatment and hence acetyl-CoA might have additional epigenetic effects on the EMT program (e.g., through histone acetylation). Also, stabilized microtubule-mediated binding of SMAD2 and acetyl-CoA level–associated SMAD7 acetylation might negatively regulate TGF-β signaling during EMT (Dong *et al.*, 2000; Xiong *et al.*, 2018). Even so, our observations suggest that therapeutic manipulation of acetate production and levels could provide the basis for treating various EMT-linked pathological conditions such as cancer.

Discoveries of the mechanism and regulation of lipid metabolism were awarded the Nobel Prize in Physiology or Medicine in 1964 (Xiong, 2018b). However, the fatty acid metabolism's role in health and disease is incompletely characterized. Recent evidence suggests that the short-chain fatty acid acetate might play a role in protection of infection (Fukuda *et al.*, 2011) and cancer cell growth arrest (Sahuri-Arisoylu *et al.*, 2021). Moreover, dietary fructose can be converted to acetate by the gut microbiota (Zhao *et al.*, 2020). It might be helpful to define how fructose and other dietary sources of acetate, such as ethanol and fermentable fibers, influence the treatment of diseases in a clinical setting. Because acetate is the predominant short-chain fatty acid generated from gut microbial fermentation (Bergman, 1990; Moffett *et al.*, 2020), our results suggest that therapeutic manipulation of microbiota-derived acetate could provide the basis for treating EMT-linked tumor progression.

MATERIALS AND METHODS

Cell culture

The human lung epithelial cancer cell line A549 cells (American Type Culture Collection) were cultured in Ham's F-12K (Kaighn's) Medium (21127022; Thermo Fisher Scientific, Waltham, MA), supplemented with 10% (vol/vol) fetal bovine serum (FBS; HyClone), 100 U/ml

FIGURE 2: Acetate mediates EMT. (A) A model for how acetate, converted to acetyl-CoA, replenishes cellular acetyl-CoA pools. (B) Relative levels of acetyl-CoA in control or acetate-treated A549 cells ($n = 3$ experiments). (C) Acetate supplementation inhibits a TGF-β1–induced EMT-associated morphological switch. Scale bar, 100 μm. (D) Western blot of phosphorylated SMAD2 (pSMAD2) in control cells or A549 cells, with or without acetate, following TGF-β1 stimulation ($n = 3$ experiments). (E, F) Western blot of SNAIL (E) and E-cadherin (F) in control cells or A549 cells, with or without acetate, following TGF-β1 stimulation ($n = 3$ experiments). (G, H) Representative immunostaining images (G) and quantification (H) of epithelial marker E-cadherin in control cells or A549 cells, with or without acetate, following TGF-β1 stimulation. (I, J) Representative microscopic images (I) and quantification (J) of cell motility in control cells or A549 cells, with or without acetate, following TGF-β1 stimulation ($n = 3$ experiments). Cell motility determined by wound closure analysis. Scale bar, 100 μm. Data represent mean ± SEM and significance via one-way ANOVA with Tukey's multiple comparison test (D–F, H, and J). *, $p < 0.05$; **, $p < 0.01$; ***, $p < 0.001$.

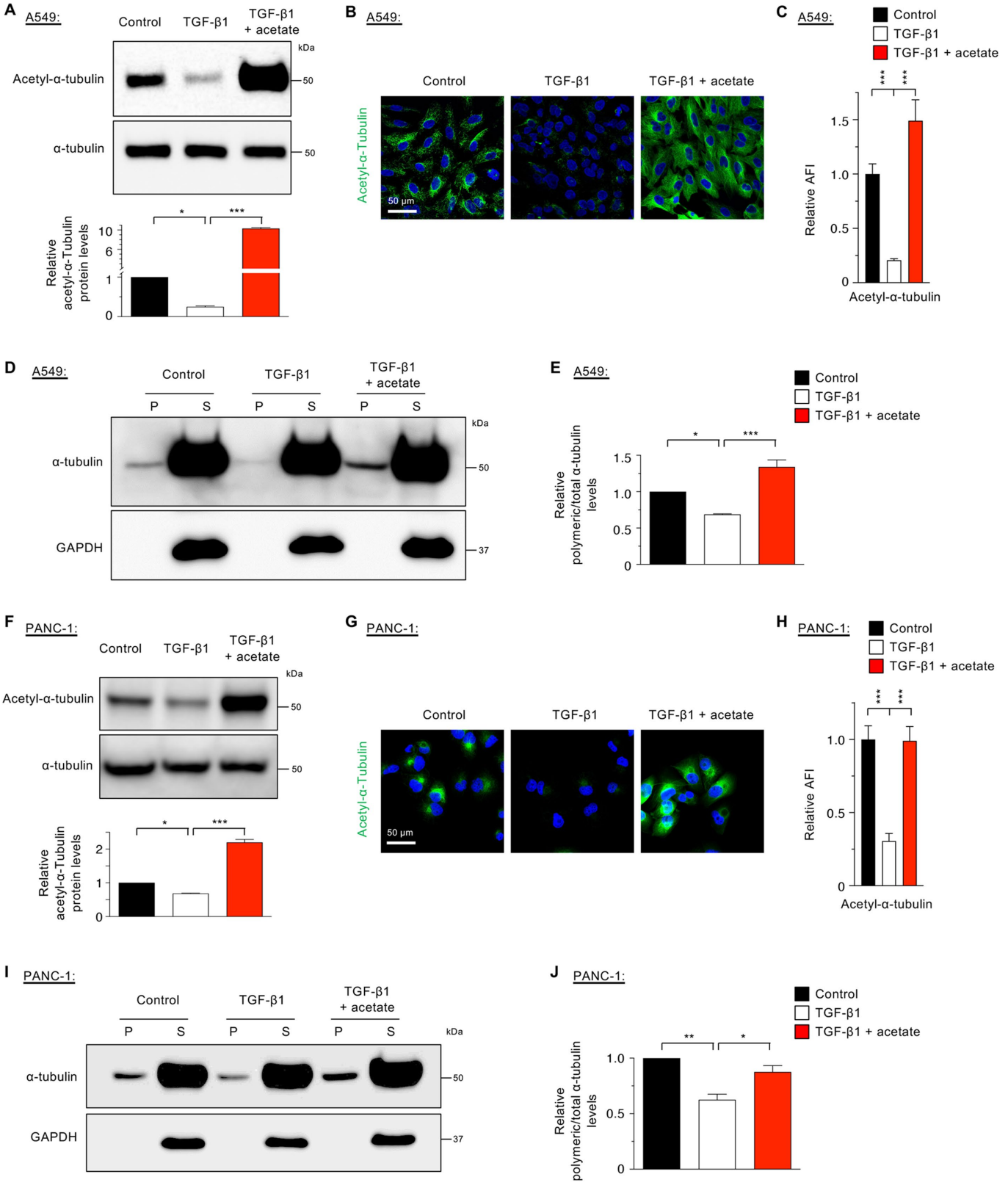

FIGURE 3: Acetate controls EMT by modulating EMT-associated α-tubulin acetylation and microtubule stability. (A) Western blot of acetyl-α-tubulin in control cells or A549 cells, with or without acetate, following TGF-β1 stimulation ($n = 3$ experiments). (B, C). Representative immunostaining images (B) and quantification (C) of acetyl-α-tubulin in control cells or A549 cells, with or without acetate, following TGF-β1 stimulation. Scale bar, 50 μm. (D, E) Representative Western blot (D) and quantification (E) of microtubule polymerization in control cells or A549 cells, with or without acetate, following TGF-β1 stimulation ($n = 3$ experiments). (F) Western blot of acetyl-α-tubulin in control cells or PANC-1 cells, with or without acetate, following TGF-β1 stimulation ($n = 3$ experiments). (G, H). Representative immunostaining

penicillin, and 100 µg/ml streptomycin (15070-063; Thermo Fisher Scientific). The human pancreatic epithelial cancer cell line PANC-1 cells (American Type Culture Collection) were cultured in DMEM (D5796; Sigma-Aldrich, Saint Louis, MO), supplemented with 10% (vol/vol) FBS (HyClone), 100 U/ml penicillin, and 100 µg/ml streptomycin (15070-063; Thermo Fisher Scientific). The mouse mammary epithelial cell line NMuMG cells (American Type Culture Collection) were cultured in DMEM (D5796; Sigma-Aldrich), supplemented with 10% (vol/vol) FBS (HyClone), 10 µg/ml insulin (91077C-100MG; Sigma-Aldrich), 100 U/ml penicillin, and 100 µg/ml streptomycin (15070-063; Thermo Fisher Scientific). All the cell lines were regularly evaluated for mycoplasma contamination using MycoAlert Mycoplasma Detection Kit (Lonza, Basel, Switzerland). Cell morphology was examined using a Nikon Eclipse Ti or TS 100 microscope (Nikon, Tokyo, Japan) and acquired images using NIS-Elements Imaging Software (version 5.21.03).

Chemicals, plasmids, and lentiviral vectors

Cells were seeded in a six-well plate and treated with 10 ng/ml TGF-β1 (240-B-010/CF; R&D Systems, Minneapolis, MN), with or without 40 mM sodium acetate (S5636; Sigma-Aldrich, Saint Louis, MO), for 2 d. The concentrations of TGF-β1 and acetate have been previously employed (Xiong *et al.*, 2018). A549 cells were treated with the microtubule destabilizer, vinorelbine (V2264-5MG; Sigma-Aldrich) at a final concentration of 100 nM, or the CDK4/6 inhibitor, palbociclib (PD 0332991; 16273; Cayman Chemical, Ann Arbor, MI) at a final concentration of 5 µM. A549 cells were incubated with the ACLY inhibitor, SB-204990 (4962; Bio-Techne, Minneapolis, MN) at a final concentration of 100 µM. After 3 h of SB-204990 treatment, Western blot measurement of SNAIL protein expression in A549 cells was performed, while E-cadherin was assessed 1 d after SB-204990 treatment. Wild-type α-tubulin (Tubulin-WT) plasmid and its mutant version with K40R (Tubulin-K40R) were used (Gao *et al.*, 2010). The lentiviral vectors for overexpression of Tubulin-WT and Tubulin-K40R were cloned in pCDH-CMV vector backbone.

Western blotting

Cells were lysed with a RIPA buffer (BP-115; Boston BioProducts, Milford, MA) containing protease inhibitor (11836170001; Roche Life Sciences, Mannheim, Germany) and phosphatase inhibitor cocktails (04906837001; Roche Life Sciences). A Pierce BCA Protein Assay Kit (23209; Thermo Fisher Scientific) was used to measure protein concentration. The protein lysates were diluted with 4× Laemmli sample buffer (1610747; Bio-Rad Laboratories, Hercules, CA) and then boiled at 95°C for 10 min. The samples were separated on Mini-PROTEAN TGX Gel (4561096; Bio-Rad Laboratories). The separated molecules were blotted onto a nitrocellulose membrane and the membrane was blocked with 5% nonfat milk for 1 h at room temperature. The membrane was probed with the primary antibody overnight at 4°C followed by a horseradish peroxidase–conjugated secondary antibody for 1 h at room temperature. The primary antibody against α-tubulin (T5168) was purchased from Sigma-Aldrich. The following primary antibodies from Cell Signaling Technology (Danvers, MA) were used: acetyl-α-tubulin (5335S), E-cadherin (3195P), pSMAD1/5 (13820P), pSMAD2 (3108S), SMAD1 (6944P), SMAD2 (5339S), SMAD5 (12534P), and SNAIL (3879S). A primary antibody against HSP60 (sc-1052) was purchased from Santa Cruz Biotechnology (Dallas, TX). A primary antibody against CPT1A (ab128568) was purchased from Abcam (Cambridge, United Kingdom). Secondary antibodies conjugated horseradish peroxidase (HRP) against mouse IgG (1706515) or rabbit IgG (1706510) were purchased from Bio-Rad Laboratories. The protein bands were detected with Clarity Western ECL Substrate (1705061; Bio-Rad Laboratories) under the ChemiDoc MP imaging system (Bio-Rad Laboratories). Image Lab Touch or Image Lab (version 6.1.0 build 7) software was used to acquire and analyze Western blot images.

FAO assay

The XF96 extracellular flux analyzer (Agilent) was used to assess A549 cells' ability to oxidize exogenous fatty acids according to a previous protocol (Xiong *et al.*, 2018) with minor modifications. The utility plate was filled with 200 µl XF Calibrant Solution (Agilent) overnight in a humidified non-CO_2 37°C incubator. A549 cells were treated with or without 10 ng/ml TGF-β1 for 2 d and seeded them on an XF96 cell culture microplate (Agilent). To analyze the oxygen consumption rate (OCR) of A549 cells with or without treatment of 10 ng/ml TGF-β1, 2×10^4 cells per well were seeded on an XF96 cell culture microplate (Agilent). Immediately before the assay, the medium was changed to FAO assay medium (111 mM NaCl, 4.7 mM KCl, 1.25 mM $CaCl_2$, 2.0 mM $MgSO_4$, 1.2 mM Na_2HPO_4, 2.5 mM glucose, 0.5 mM carnitine, and 5 mM HEPES), adjusted to pH 7.4. The cells were subsequently maintained in a non-CO_2 incubator for approximately 45 min to 1 h at 37°C. After that, the XF Palmitate-BSA (bovine serum albumin) FAO substrates (102720-100; Agilent), palmitate-BSA (166.7 µM palmitate conjugated with 28.3 mM BSA) or BSA (28.3 mM BSA) was added. OCR was measured using the XF Cell Mito Stress Test and the data was analyzed using Wave software (version 2.4.0; Agilent).

High-performance liquid chromatography analysis of acetyl-CoA

Acetyl-CoA levels were measured in A549 cells with CPT1A overexpression or treated with 10 ng/ml TGF-β1 as previously described (Xiong *et al.*, 2018). The cells were resuspended in a 5% 5-sulfosalicylic acid (S3147-100G; Sigma-Aldrich) solution. Samples were frozen in liquid nitrogen and thawed on ice twice to permeabilize the cells. After centrifugation, the supernatant was filtered with Ultrafree-MC LH Centrifugal Filter (UFC30LH25; Millipore), and then transferred into SUN-SRi Glass Microsampling Vials (14-823-359; Thermo Fisher Scientific) with SUN-SRi 11 mm Snap Caps (14-823-379; Thermo Fisher Scientific). Acetyl-CoA was separated with an Agilent 1100 HPLC (high-performance liquid chromatography) with a fluorescence detector (Agilent) on a Luna 3 µm C18(2) column (150 × 4.6 mm, 3 µm; Phenomenex, Torrance, CA). Data was analyzed using ChemoStation software Rev. A.10.01 (Agilent).

Immunofluorescence and FAOBlue staining

Cells were seeded in a Nunc Lab-Tek II 8-Chamber Slide (154534; Thermo Fisher Scientific) and treated them with TGF-β1, with or

images (G) and quantification (H) of acetyl-α-tubulin in control cells or PANC-1 cells, with or without acetate, following TGF-β1 stimulation. Scale bar, 50 µm. (I, J) Representative Western blot (I) and quantification (J) of microtubule polymerization in control cells or PANC-1 cells, with or without acetate, following TGF-β1 stimulation ($n = 3$ experiments). Data represent mean ± SEM and significance via one-way ANOVA with Tukey's multiple comparison test (A, C, E, F, H, and J). *, $p < 0.05$; **, $p < 0.01$; ***, $p < 0.001$.

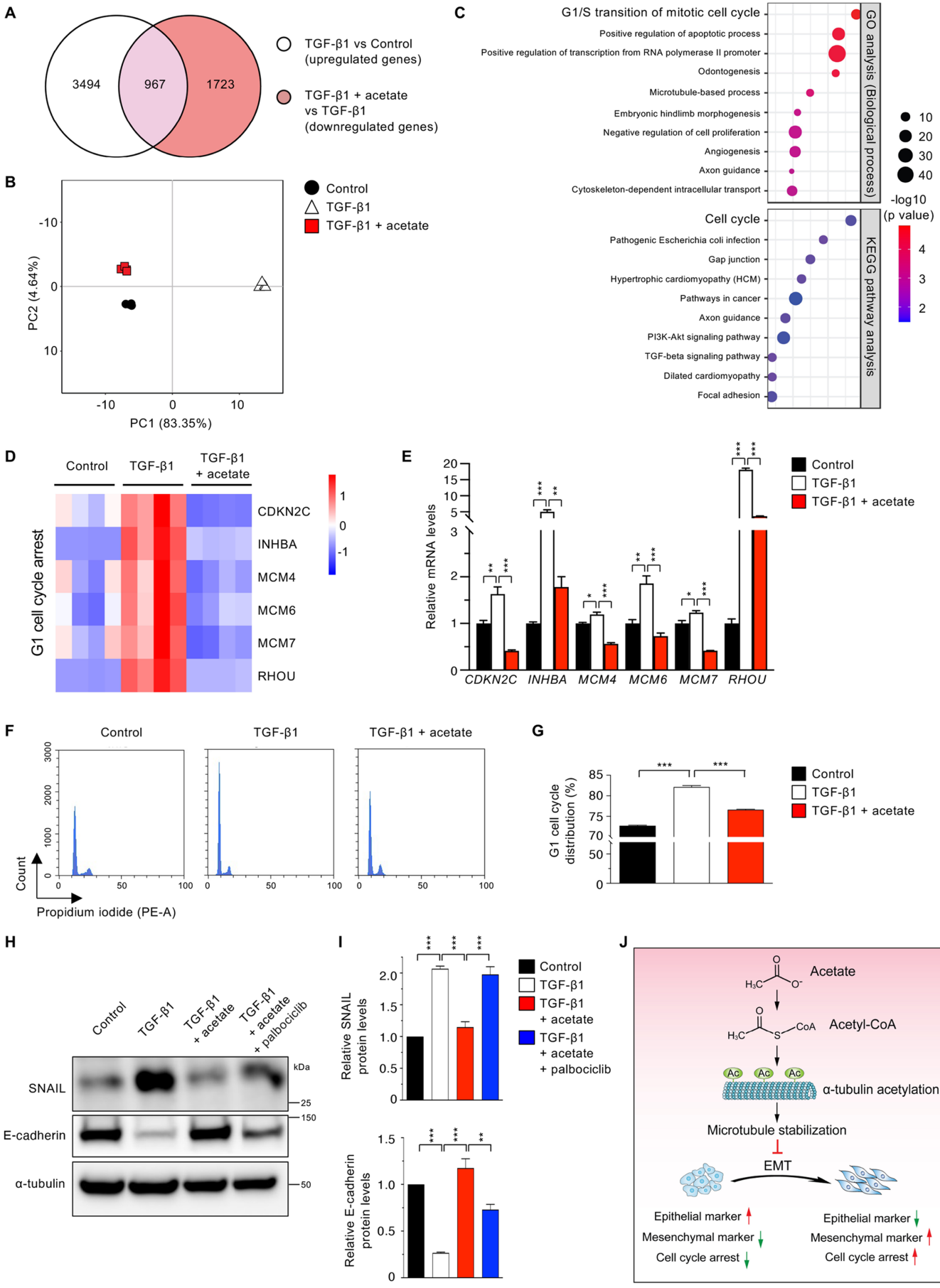
A
3494
967
1723
TGF-β1 vs Control
(upregulated genes)
TGF-β1 + acetate
vs TGF-β1
(downregulated genes)
B
Control
TGF-β1
TGF-β1 + acetate
PC2 (4.64%)
PC1 (83.35%)
C
G1/S transition of mitotic cell cycle
Positive regulation of apoptotic process
Positive regulation of transcription from RNA polymerase II promoter
Odontogenesis
Microtubule-based process
Embryonic hindlimb morphogenesis
Negative regulation of cell proliferation
Angiogenesis
Axon guidance
Cytoskeleton-dependent intracellular transport
GO analysis (Biological process)
Cell cycle
Pathogenic Escherichia coli infection
Gap junction
Hypertrophic cardiomyopathy (HCM)
Pathways in cancer
Axon guidance
PI3K-Akt signaling pathway
TGF-beta signaling pathway
Dilated cardiomyopathy
Focal adhesion
KEGG pathway analysis
-log10
(p value)
D
Control
TGF-β1
TGF-β1
+ acetate
G1 cell cycle arrest
CDKN2C
INHBA
MCM4
MCM6
MCM7
RHOU
E
Relative mRNA levels
Control
TGF-β1
TGF-β1 + acetate
CDKN2C
INHBA
MCM4
MCM6
MCM7
RHOU
F
Control
TGF-β1
TGF-β1 + acetate
Count
Propidium iodide (PE-A)
G
G1 cell cycle
distribution (%)
Control
TGF-β1
TGF-β1 + acetate
H
Control
TGF-β1
TGF-β1
+ acetate
TGF-β1
+ acetate
+ palbociclib
kDa
SNAIL
E-cadherin
α-tubulin
I
Relative SNAIL
protein levels
Relative E-cadherin
protein levels
Control
TGF-β1
TGF-β1
+ acetate
TGF-β1
+ acetate
+ palbociclib
J
Acetate
Acetyl-CoA
α-tubulin acetylation
Microtubule stabilization
EMT
Epithelial marker
Mesenchymal marker
Cell cycle arrest
Epithelial marker
Mesenchymal marker
Cell cycle arrest

without 40 mM sodium acetate, for 2 d. The cells were fixed with 4% paraformaldehyde (28908; Thermo Fisher Scientific) for 20 min at room temperature and then permeabilized them with 0.5% Triton X-100 (1610407; Bio-Rad Laboratories) for 15 min at room temperature. For E-cadherin staining, nonpermeabilized cells were used and analyzed. The cells were blocked with 3% BSA (700-107P; Geminibio, West Sacramento, CA) in PBS for 1 h. The cells were incubated with acetyl-α-tubulin (5335S; Cell Signaling Technology) and E-cadherin (3195P; Cell Signaling Technology) primary antibodies overnight at 4°C. Then the cells were incubated with anti-rabbit secondary antibodies conjugated to Alexa Fluor 488 (A11034; Thermo Fisher Scientific) for 1 h at room temperature. The nuclei were stained with Hoechst 33342 (H3570; Thermo Fisher Scientific) for 5 min at room temperature. The cells were mounted with Immumount (9990402; Epredia, Kalamazoo, MI). For FAOBlue staining-based analysis of FAO, A549 cells were seeded in a four-well confocal dish and incubated them overnight. The cells were treated with 10 ng/ml TGF-β1, with or without 40 mM sodium acetate, for 2 d before adding FAOBlue (FDV-0033; Funakoshi, Tokyo, Japan). Following the manufacturer's instructions (Uchinomiya *et al.*, 2020), the culture medium was removed and then the cells were washed twice with HEPES-buffered saline (HBS). Then, 5 μM FAOBlue in HBS was added to the cells for 30 min of incubation at 37°C. The cells were imaged under Nikon Eclipse Ti2 confocal microscope and acquired images using NIS-Elements Imaging Software (version 5.21.03). Average fluorescent intensity was determined by dividing the overall mean fluorescence intensity by the area of the cell from at least 10 cells and quantified using Image J (version 1.53k).

Wound-healing assay

Cells were seeded in a six-well plate at a density of 2×10^5 A549 cells/well or 4×10^5 PANC-1 cells/well and incubated them overnight. For A549 cells, the cells were treated with 10 ng/ml TGF-β1, with or without 40 mM sodium acetate, for 2 d before creating the wound area with a 10-μl pipette tip. For PANC-1 cells, the wound area was created by a 10-μl pipette tip and the cells were treated with 10 ng/ml TGF-β1, with or without 40 mM sodium acetate, for 24 h. The cell image was acquired under a Nikon Eclipse Ti microscope, using NIS-Elements Imaging Software (version 5.21.03). Cell migration was quantified using Image J based on the relative wound distance.

Cell cycle assay

A549 cells were seeded in a six-well plate and treated them with 10 ng/ml TGF-β1, with or without 40 mM sodium acetate, for 2 d. Then the cells were harvested, washed with PBS, and fixed with cold 70% ethanol overnight at −20°C. The cold 70% ethanol was added in a dropwise manner. The fixed cells were washed with PBS and suspended in 0.5 ml PBS containing 50 μg/ml propidium iodide (PI), 0.1 mg/ml RNase A, and 0.1% Triton X-100 for 30 min at 37°C. Then the cells were washed with cell staining/washing buffer (420201; BioLegend) three times and their cell cycle was analyzed under a CytoFLEX Flow Cytometer (Beckman Coulter, Brea, CA). The software CytExpert for CytoFLEX Acquisition and Analysis was used to acquire and analyze cell cycle data.

Real-time qRT-PCR

A549 cells were seeded in a six-well dish and treated them with 10 ng/ml TGF-β1, with or without 40 mM sodium acetate, for 2 d. Total RNA was extracted using Direct-zol RNA Miniprep Plus (R2072; ZYMO RESEARCH, Irvine, CA). Complementary DNA was synthesized using an iScript cDNA Synthesis Kit (1708891; Bio-Rad Laboratories). Real-time qPCR was performed on a CFX Connect real-time PCR detection system (Bio-Rad) using a THUNDERBIRD SYBR qPCR mix (Toyobo; QPS-201) or THUNDERBIRD Next SYBR qPCR mix (Toyobo; QPX-201), according to the manufacturer's instructions. Data was using the comparative cycling threshold ($\Delta\Delta Ct$) method. Bio-Rad CFX Maestro was used to acquire the data and the comparative CT ($2^{-\Delta\Delta}$Ct) method was used to quantify relative mRNA level. The primers were synthesized and purified by Integrated DNA Technologies (Coralville, IA). The following primers were used to detect gene expression: 18S rRNA, forward primer, 5′-GTAACCCGTTGAACCCCATT-3′, and reverse primer, 5′-CCATCCAATCGGTAGTAGCG-3′; human *ACTA2*, forward primer, 5′-CAGCCAAGCACTGTCAGG-3′, and reverse primer, 5′-CCAGAGCCATTGTCACACAC-3′; human *CDH1*, forward primer, 5′-CCGCTGGCGTCTGTAGGAA-3′, and reverse primer, 5′-AGGGCTCTTTGACCACCGCTCTC-3′; human *CDH2*, forward primer, 5′-GTGCATGAAGGACAGCCTCT-3′, and reverse primer, 5′-CCACCTTAAAATCTGCAGGC-3′; human *CDKN2C*, forward primer, 5′-GTAAACGTCAATGCACAAAATGG-3′, and reverse primer, 5′-AGTTCGGTCTTTCAAATCGGG-3′; human *EPCAM*, forward primer, 5′-AATCGTCAATGCCAGTGTACTT-3′, and reverse primer, 5′-TCTCATCGCAGTCAGGATCATAA-3′; human *INHBA*, forward primer, 5′-ACGGGTATGTGGAGATAGAGG-3′, and reverse primer, 5′-TGGAAATCTCGAAGTGCAGC-3′; human *KRT18*, forward primer, 5′-TCGCAAATACTGTGGACAATGC-3′, and reverse primer, 5′-GCAGTCGTGTGATATTGGTGT-3′; human *KRT19*, forward primer, 5′-AACGGCGAGCTAGAGGTGA-3′, and reverse primer, 5′-GGATGGTCGTGTAGTAGTGGC-3′; human *MCM4*, forward primer, 5′-TTCTTTGACCGTTACCCTGAC-3′, and reverse primer,

FIGURE 4: Acetate regulates EMT-associated G1 cell cycle arrest. (A) RNA-Seq Venn diagram shows common differentially expressed genes of TGF-β1–activated genes and acetate-suppressed genes. (B) PCA of common differentially expressed genes of TGF-β1–activated genes and acetate-suppressed genes from RNA-Seq data of control cells or the A549 cells treated with or without acetate following TGF-β1 stimulation. Each stimulation was performed in quadruplicate. (C) RNA-Seq bubble plot depicts top 10 enriched GO biological processes and top 10 KEGG pathways for the common differentially expressed genes of TGF-β1–activated genes and acetate-suppressed genes from RNA-Seq data of control cells or A549 cells treated with or without acetate following TGF-β1 stimulation. (D) Heatmap of RNA-Seq data for key genes associated with G1 cell cycle arrest. (E) mRNA levels by qRT-PCR of genes associated with G1 cell cycle arrest in control cells or A549 cells treated with or without acetate following TGF-β1 stimulation. (F, G) Flow cytometric analysis (F) and quantification (G) of cell cycle progression in control cells or A549 cells, with or without acetate, following TGF-β1 stimulation ($n = 3$ experiments). *x*-axis represents propidium iodine and *y*-axis represents cell count. (H, I) The CDK4/6 inhibitor palbociclib inhibits the effects of acetate on EMT. (J) Model for how acetate, converted to acetyl-CoA, inhibits the EMT program through regulation of α-tubulin acetylation, microtubule stability, and cell cycle arrest. Data represent mean ± SEM and significance via one-way ANOVA with Tukey's multiple comparison test (E and G). **, $p < 0.01$; ***, $p < 0.001$.

5′-GGGATGTCCTGATCACCATG-3′; human *MCM6*, forward primer, 5′-GTGATCAGGGATGTAGAACAGC-3′, and reverse primer, 5′-AGCTTGGGTCTCTTGAATACG-3′; human *MCM7*, forward primer, 5′-GATGCCACCTATACTTCTGCC-3′, and reverse primer, 5′-TCCTTTGACATCTCCATTAGCC-3′; human *RHOU*, forward primer, 5′-GTACATCCCTACTGCCTTCG-3′, and reverse primer, 5′-AGGAAGATGTCTGTGTTGGTG-3′; human *RPL7*, forward primer, 5′-CAAGGCTTCGATTAACATGCTGA-3′, and reverse primer, 5′-GCCATAACCACGCTTGTAGATT-3′; human *SNAI1*, forward primer, 5′-CTCTAGGCCCTGGCTGCTAC-3′, and reverse primer, 5′-TCTGAGTGGGTCTGGAGGTG-3′; human *VIM*, forward primer, 5′-CTTCAGAGAGAGGAAGCCGA-3′, and reverse primer, 5′-ATTCCACTTTGCGTTCAAGG.

Microtubule stability assay

Microtubule stability assay was performed based on a previous report (Nishida *et al.*, 2005). Cells were treated with 10 ng/ml TGF-β1, with or without 40 mM sodium acetate, for 2 d and then suspended in 200 µl of extraction buffer containing 0.1 M PIPES, pH 7.1, 1 mM $MgSO_4$, 1 mM EGTA, 2 M glycerol, 0.1% Triton X-100, and a protease inhibitor and phosphatase inhibitor cocktail. The cell lysates were on ice for 15 min, and then centrifuged at 15,000 rpm for 15 min at 4°C. The supernatant containing soluble tubulin was collected. The remaining pellet was resuspended in a lysis buffer containing 25 mM Tris-HCl, pH 7.4, 0.4 M NaCl, and 0.5% SDS. The sample was boiled for 10 min at 95°C, then centrifuged at 15,000 rpm for 5 min at room temperature. The supernatant containing polymeric tubulin was then collected. The soluble (S) and polymerized (P) tubulins were subjected to SDS–PAGE, and then detected by Western blot using an anti–α-tubulin antibody. An anti-GAPDH antibody (5174S; Cell Signaling Technology) was used as a loading control. The microtubule polymerization was quantified based on the ratio of polymerized (P) tubulin to total tubulin (P + S) using Image Lab software (version 6.1.0 build 7).

RNA sequencing analysis

Total RNA was extracted from control A549 cells and cells treated with TGF-β1, with or without 40 mM sodium acetate, using the RNeasy Mini Kit (74106; Qiagen, Germany). The sequencing libraries were constructed from 100–500 ng of total RNA using Illumina's TruSeq Stranded Total RNA kit with Ribo-Zero, following the manufacturer's instructions. The fragment size of RNA-Seq libraries was verified using the Agilent 2100 Bioanalyzer (Agilent) and the concentrations were determined using a Qubit instrument (Thermo Fisher Scientific). The libraries were then loaded onto Illumina HiSeq 3000 (Illumina, San Diego, CA) for 2 × 75 base pair paired-end read sequencing. The fastq files were generated using bcl2fastq software for further analysis. The data were analyzed as previously described (Houston *et al.*, 2020) with minor modifications. Briefly, quality confirmed RNA-Seq reads from each library were aligned and mapped with HISAT2 (Kim *et al.*, 2015). Only uniquely mapped paired-end reads were used for subsequent analyses. FeatureCounts (Liao *et al.*, 2014) was employed for gene-level abundance estimation. Differential expression analysis was performed using the open-source Limma R package (Ritchie *et al.*, 2015). Limma-voom was used to implement gene-wise linear modeling, which processes the read counts into log2 counts per million (logCPM) with associated precision weights. The logCPM values between samples were normalized using a trimmed mean of M-values. We adjusted for multiple testing by reporting the FDR q values for each feature. We declared features with $q < 5\%$ as having genome-wide significance. We identified filtered gene sets as up-regulated or down-regulated ($\log_2FC > 0.5$ or < -0.5, $p < 0.05$) in paired samples. We selected the common differentially expressed genes of TGF-β1–activated genes and acetate-suppressed genes using the Venn diagram from RNA-Seq data of control cells or the A549 cells (treated with or without acetate), following TGF-β1 stimulation. We performed each stimulation in quadruplicate. We subjected genes showing differential expression to the GO analysis using the Web-based tool, DAVID v6.8 (The Database for Annotation, Visualization, and Integrated Discovery, National Institute of Allergy and Infectious Diseases, National Institutes of Health [NIH]), for the functional annotation of transcriptome profiles. We performed the analyses of RNA-Seq PCA, bubble plot, and heatmap using an R programming environment (version 4.0.2). The RNA-Seq data were deposited in the NCBI's Gene Expression Omnibus repository with the accession number GSE197132.

Statistical analysis

Statistical data differences were determined between control and test groups using unpaired two-sided Student's *t* tests using GraphPad Prism 9 (version 9.3.1; GraphPad Software, La Jolla, CA) unless otherwise stated. Data were represented as the mean ± standard error of the mean (SEM) and p values < 0.05 were considered significant.

ACKNOWLEDGMENTS

This work was supported by NIH Grant no. K22HL-146793 to J.X. We are grateful to Timothy F. Osborne for critical reading of this manuscript, to members of Finkel lab for valuable discussion and technical support, to Ana Gomes for the NMuMG cell culture, to Duck-Yeon Lee at the NHLBI Biochemistry Core for HPLC instrumentation and calibration for acetyl-CoA, and to the NHLBI Cores (Bioinformatics and Computational Biology Core, and DNA Sequencing and Genomics Core) for experimental support.

REFERENCES

Akalay I, Janji B, Hasmim M, Noman MZ, Andre F, De Cremoux P, Bertheau P, Badoual C, Vielh P, Larsen AK, *et al.* (2013). Epithelial-to-mesenchymal transition and autophagy induction in breast carcinoma promote escape from T-cell-mediated lysis. Cancer Res 73, 2418–2427.

Balmer ML, Ma EH, Bantug GR, Grahlert J, Pfister S, Glatter T, Jauch A, Dimeloe S, Slack E, Dehio P, *et al.* (2016). Memory $CD8^+$ T cells require increased concentrations of acetate induced by stress for optimal function. Immunity 44, 1312–1324.

Bergman EN (1990). Energy contributions of volatile fatty acids from the gastrointestinal tract in various species. Physiol Rev 70, 567–590.

Blajeski AL, Phan VA, Kottke TJ, Kaufmann SH (2002). G_1 and G_2 cell-cycle arrest following microtubule depolymerization in human breast cancer cells. J Clin Invest 110, 91–99.

Cai L, Sutter BM, Li B, Tu BP (2011). Acetyl-CoA induces cell growth and proliferation by promoting the acetylation of histones at growth genes. Mol Cell 42, 426–437.

Canovas NS, Manzoni M, Pizzi M, Mandato E, Carrino M, Quotti Tubi L, Zambello R, Adami F, Visentin A, BarilàG, *et al.* (2018). The small GTPase RhoU lays downstream of JAK/STAT signaling and mediates cell migration in multiple myeloma. Blood Cancer J 8, 20.

Chei S, Oh HJ, Song JH, Seo YJ, Lee K, Lee BY (2019). Magnolol suppresses TGF-β-induced epithelial-to-mesenchymal transition in human colorectal cancer cells. Front Oncol 9, 752.

David CJ, Massague J (2018). Contextual determinants of TGFβ action in development, immunity, and cancer. Nat Rev Mol Cell Biol 19, 419–435.

Derynck R, Turley SJ, Akhurst RJ (2021). TGFβ biology in cancer progression and immunotherapy. Nat Rev Clin Oncol 18, 9–34.

Dong C, Li Z, Alvarez R, Jr., Feng XH, Goldschmidt-Clermont PJ. (2000). Microtubule binding to Smads may regulate TGFβ activity. Mol Cell 5, 27–34.

Dongre A, Weinberg RA (2019). New insights into the mechanisms of epithelial-mesenchymal transition and implications for cancer. Nat Rev Mol Cell Biol 20, 69–84.

Eckert MA, Lwin TM, Chang AT, Kim J, Danis E, Ohno-Machado L, Yang J. (2011). Twist1-induced invadopodia formation promotes tumor metastasis. Cancer Cell 19, 372–386.
Fukuda S, Toh H, Hase K, Oshima K, Nakanishi Y, Yoshimura K, Tobe T, Clarke JM, Topping DL, Suzuki T, *et al*. (2011). Bifidobacteria can protect from enteropathogenic infection through production of acetate. Nature 469, 543–547.
Gao YS, Hubbert CC, Yao TP (2010). The microtubule-associated histone deacetylase 6 (HDAC6) regulates epidermal growth factor receptor (EGFR) endocytic trafficking and degradation. J Biol Chem 285, 11219–11226.
Greenburg G, Hay ED (1982). Epithelia suspended in collagen gels can lose polarity and express characteristics of migrating mesenchymal cells. J Cell Biol 95, 333–339.
Gu S, Liu Y, Zhu B, Ding K, Yao TP, Chen F, Zhan L, Xu P, Ehrlich M, Liang T, *et al*. (2016). Loss of α-tubulin acetylation is associated with TGF-β-induced epithelial-mesenchymal transition. J Biol Chem 291, 5396–5405.
Guan KL, Jenkins CW, Li Y, Nichols MA, Wu X, O'Keefe CL, Matera AG, Xiong Y (1994). Growth suppression by p18, a p16INK4/MTS1- and p14INK4B/MTS2-related CDK6 inhibitor, correlates with wild-type pRb function. Genes Dev 8, 2939–2952.
Hanahan D (2022). Hallmarks of cancer: new dimensions. Cancer Discov 12, 31–46.
Hirai H, Roussel MF, Kato JY, Ashmun RA, Sherr CJ (1995). Novel INK4 proteins, p19 and p18, are specific inhibitors of the cyclin D-dependent kinases CDK4 and CDK6. Mol Cell Biol 15, 2672–2681.
Houston R, Sekine S, Calderon MJ, Seifuddin F, Wang G, Kawagishi H, Malide DA, Li Y, Gucek M, Pirooznia M, *et al*. (2020). Acetylation-mediated remodeling of the nucleolus regulates cellular acetyl-CoA responses. PLoS Biol 18, e3000981.
Houten SM, Violante S, Ventura FV, Wanders RJ (2016). The biochemistry and physiology of mitochondrial fatty acid β-oxidation and its genetic disorders. Annu Rev Physiol 78, 23–44.
Iwano M, Plieth D, Danoff TM, Xue C, Okada H, Neilson EG (2002). Evidence that fibroblasts derive from epithelium during tissue fibrosis. J Clin Invest 110, 341–350.
Jiang L, Si T, Yu M, Zeng X, Morse HC, 3rd, Lu Y, Ouyang G, Zhou JX (2018). The tumor suppressive role of inhibin βA in diffuse large B-cell lymphoma. Leuk Lymphoma 59, 1202–1212.
Kim D, Langmead B, Salzberg SL (2015). HISAT: a fast spliced aligner with low memory requirements. Nat Methods 12, 357–360.
Kudo-Saito C, Shirako H, Takeuchi T, Kawakami Y (2009). Cancer metastasis is accelerated through immunosuppression during Snail-induced EMT of cancer cells. Cancer Cell 15, 195–206.
Labib K, Kearsey SE, Diffley JF (2001). MCM2-7 proteins are essential components of prereplicative complexes that accumulate cooperatively in the nucleus during G1-phase and are required to establish, but not maintain, the S-phase checkpoint. Mol Biol Cell 12, 3658–3667.
Lee JV, Carrer A, Shah S, Snyder NW, Wei S, Venneti S, Worth AJ, Yuan ZF, Lim HW, Liu S, *et al*. (2014). Akt-dependent metabolic reprogramming regulates tumor cell histone acetylation. Cell Metab 20, 306–319.
Liao Y, Smyth GK, Shi W (2014). featureCounts: an efficient general-purpose program for assigning sequence reads to genomic features. Bioinformatics 30, 923–930.
Moffett JR, Puthillathu N, Vengilote R, Jaworski DM, Namboodiri AM (2020). Acetate revisited: a key biomolecule at the nexus of metabolism, epigenetics, and oncogenesis - part 2: acetate and ACSS2 in health and disease. Front Physiol 11, 580171.
Moussaieff A, Rouleau M, Kitsberg D, Cohen M, Levy G, Barasch D, Nemirovski A, Shen-Orr S, Laevsky I, Amit M, *et al*. (2015). Glycolysis-mediated changes in acetyl-CoA and histone acetylation control the early differentiation of embryonic stem cells. Cell Metab 21, 392–402.
Nakaya Y, Sukowati EW, Wu Y, Sheng G (2008). RhoA and microtubule dynamics control cell-basement membrane interaction in EMT during gastrulation. Nat Cell Biol 10, 765–775.
Nieto MA, Huang RY, Jackson RA, Thiery JP (2016). EMT: 2016. Cell 166, 21–45.
Nishida K, Yamasaki S, Ito Y, Kabu K, Hattori K, Tezuka T, Nishizumi H, Kitamura D, Goitsuka R, Geha RS, *et al*. (2005). FcεRI-mediated mast cell degranulation requires calcium-independent microtubule-dependent translocation of granules to the plasma membrane. J Cell Biol 170, 115–126.
Pietrocola F, Galluzzi L, Bravo-San Pedro JM, Madeo F, Kroemer G. (2015). Acetyl coenzyme A: a central metabolite and second messenger. Cell Metab 21, 805–821.
Ritchie ME, Phipson B, Wu D, Hu Y, Law CW, Shi W, Smyth GK (2015). *limma* powers differential expression analyses for RNA-sequencing and microarray studies. Nucleic Acids Res 43, e47.
Sahuri-Arisoylu M, Mould RR, Shinjyo N, Bligh SWA, Nunn AVW, Guy GW, Thomas EL, Bell JD (2021). Acetate induces growth arrest in colon cancer cells through modulation of mitochondrial function. Front Nutr 8, 588466.
Schafer ZT, Grassian AR, Song L, Jiang Z, Gerhart-Hines Z, Irie HY, Gao S, Puigserver P, Brugge JS (2009). Antioxidant and oncogene rescue of metabolic defects caused by loss of matrix attachment. Nature 461, 109–113.
Schmierer B, Hill CS (2007). TGFβ-SMAD signal transduction: molecular specificity and functional flexibility. Nat Rev Mol Cell Biol 8, 970–982.
Schoors S, Bruning U, Missiaen R, Queiroz KC, Borgers G, Elia I, Zecchin A, Cantelmo AR, Christen S, Goveia J, *et al*. (2015). Fatty acid carbon is essential for dNTP synthesis in endothelial cells. Nature 520, 192–197.
Schug ZT, Peck B, Jones DT, Zhang Q, Grosskurth S, Alam IS, Goodwin LM, Smethurst E, Mason S, Blyth K, *et al*. (2015). Acetyl-CoA synthetase 2 promotes acetate utilization and maintains cancer cell growth under metabolic stress. Cancer Cell 27, 57–71.
Uchinomiya S, Matsunaga N, Kamoda K, Kawagoe R, Tsuruta A, Ohdo S, Ojida A (2020). Fluorescence detection of metabolic activity of the fatty acid beta oxidation pathway in living cells. Chem Commun (Camb) 56, 3023–3026.
Vicovac L, Aplin JD (1996). Epithelial-mesenchymal transition during trophoblast differentiation. Acta Anat (Basel) 156, 202–216.
von Gise A, Pu WT (2012). Endocardial and epicardial epithelial to mesenchymal transitions in heart development and disease. Circ Res 110, 1628–1645.
Wellen KE, Hatzivassiliou G, Sachdeva UM, Bui TV, Cross JR, Thompson CB (2009). ATP-citrate lyase links cellular metabolism to histone acetylation. Science 324, 1076–1080.
Wong BW, Wang X, Zecchin A, Thienpont B, Cornelissen I, Kalucka J, Garcia-Caballero M, Missiaen R, Huang H, Bruning U, *et al*. (2017). The role of fatty acid β-oxidation in lymphangiogenesis. Nature 542, 49–54.
Xiong J (2018a). Fatty acid oxidation in cell fate determination. Trends Biochem Sci 43, 854–857.
Xiong J (2018b). A 'nobel' look at metabolism. Trends Endocrinol Metab 29, 809–813.
Xiong J, Kawagishi H, Yan Y, Liu J, Wells QS, Edmunds LR, Fergusson MM, Yu ZX, Rovira II, Brittain EL, *et al*. (2018). A metabolic basis for endothelial-to-mesenchymal transition. Mol Cell 69, 689–698.e687.
Yang J, Antin P, Berx G, Blanpain C, Brabletz T, Bronner M, Campbell K, Cano A, Casanova J, Christofori G, *et al*. (2020). Guidelines and definitions for research on epithelial-mesenchymal transition. Nat Rev Mol Cell Biol 21, 341–352.
Ye X, Weinberg RA (2015). Epithelial-mesenchymal plasticity: a central regulator of cancer progression. Trends Cell Biol 25, 675–686.
Yun T, Ko HR, Jo DG, Park KW, Cho SW, Kim J, Ahn JY (2021). Inhibitor of DNA binding 2 (Id2) mediates microtubule polymerization in the brain by regulating αK40 acetylation of α-tubulin. Cell Death Discov 7, 257.
Zeisberg EM, Tarnavski O, Zeisberg M, Dorfman AL, McMullen JR, Gustafsson E, Chandraker A, Yuan X, Pu WT, Roberts AB, *et al*. (2007a). Endothelial-to-mesenchymal transition contributes to cardiac fibrosis. Nat Med 13, 952–961.
Zeisberg M, Yang C, Martino M, Duncan MB, Rieder F, Tanjore H, Kalluri R (2007b). Fibroblasts derive from hepatocytes in liver fibrosis via epithelial to mesenchymal transition. J Biol Chem 282, 23337–23347.
Zhao S, Jang C, Liu J, Uehara K, Gilbert M, Izzo L, Zeng X, Trefely S, Fernandez S, Carrer A, *et al*. (2020). Dietary fructose feeds hepatic lipogenesis via microbiota-derived acetate. Nature 579, 586–591.